ЖЭТФ, 2007, том 131, вып. 6, стр. 1073–1080

DYNAMIC PHASE TRANSITION IN THE KINETIC SPIN-1 BLUME – CAPEL MODEL: PHASE DIAGRAMS IN THE TEMPERATURE AND CRYSTAL-FIELD INTERACTION PLANE

M. Keskin**, *O. Canko

Department of Physics, Erciyes University
38039, Kayseri, Turkey

Ü. Temizer

Department of Physics, Bozok University
66100, Yozgat, Turkey

Received December 6, 2006

Within a mean-field approach, we study the stationary states of the kinetic spin-1 Blume – Capel model in presence of a time-dependent oscillating external magnetic field. We use the Glauber-type stochastic dynamics to describe the time evolution of the system and obtain the mean-field dynamic equation of the motion. The dynamic phase transition points are calculated and phase diagrams are presented in the temperature and crystal-field interaction plane. According to the values of the magnetic field amplitude, we find three fundamental types of phase diagrams in which they exhibit a dynamic tricritical point and only two of them a dynamic zero-temperature critical point.

PACS: 05.50.+q, 05.70.Fh, 64.60.Ht, 75.10.Hk

1. INTRODUCTION

The physics of equilibrium phase transitions is now rather well understood (see, e.g., [1]) within the framework of equilibrium statistical physics. But the mechanism behind the nonequilibrium or dynamic phase transitions (DPT) has not yet been explored rigorously, and basic phenomenology is still undeveloped. Hence, further efforts on these challenging time-dependent problems, especially calculating the DPT points and constructing the phase diagram, must be rewarding in the future. The DPT was first found in a study within a mean-field approach to the stationary states of the kinetic spin-1/2 Ising model under a time-dependent oscillating field [2, 3], by using a Glauber-type stochastic dynamics [4], and it was followed by the Monte-Carlo simulation, which allows the microscopic fluctuations, research of kinetic spin-1/2 Ising models [5–8], as well as further mean-field studies [9]. Moreover, Tutu and Fujiwara [10] developed a systematic method for obtaining the phase diagrams in DPTs and constructed the general theory of DPTs near the transition point based on the mean-field description such as Landau's general treatment of equilibrium phase transitions. The DPT has also been found within the one-dimensional kinetic spin-1/2 Ising model with boundaries [11]. Recent research on the DPT is widely extended to more complex systems such as vector-type order parameter systems, e.g., the Heisenberg spin systems [12], the XY model [13], the Ziff – Gulari – Barshad model for CO oxidation with CO desorption to periodic variation of the CO pressure [14], the mixed-spin Ising model, e.g., the kinetics of the mixed spin-1/2 and spin-1 Ising models [15], the kinetic spin-1 Ising systems [16], and the kinetic spin-3/2 Ising systems [17]. We also mention that experimental evidences for the DPT has been found in highly anisotropic (Ising-like) and ultrathin Co/Cu(001) ferromagnetic films [18] and in ferroic systems (ferromagnets, ferroelectrics, and ferroelastics) with pinned domain walls [19].

Recently [20], we used the mean-field approach to study stationary states of the kinetic spin-1 Blume – Capel model with the help of the Glauber stochastic

*E-mail: keskin@erciyes.edu.tr

dynamics in presence of a time-dependent oscillating external magnetic field. Especially, we investigated the behavior of the time dependence of the magnetization and the behavior of the average magnetization in a period as functions of the reduced temperature and reduced external magnetic field and calculated the DPT points. We only presented the phase diagrams in the reduced magnetic field amplitude (h) and reduced temperature (T) plane and obtained five different phase-diagram topologies. We also calculated the Lyapunov exponent to verify the stability of a solution and the DPT points. On the other hand, one should study phase diagrams of the dynamic phase boundaries in the temperature and crystal field interaction plane. Therefore, the aim of this paper is to present the phase diagrams of the kinetic spin-1 Blume–Capel model in presence of a time-varying (sinusoidal) magnetic field in the reduced temperature and crystal-field interaction plane by using the Glauber stochastic dynamics.

The outline of this paper is as follows. In Sec. 2, the spin-1 Blume–Capel model is presented briefly and the derivation of the mean-field dynamic equations of motion is given by using a Glauber-type stochastic dynamics in the presence of a time-dependent oscillating external magnetic field. In Sec. 3, the DPT points are calculated, and the obtained phase diagrams are presented and discussed in the reduced temperature and crystal field interaction plane. A summary is given in Sec. 4.

2. THE MODEL AND THE DERIVATION OF MEAN-FIELD DYNAMIC EQUATION OF MOTION

The spin-1 Ising model with a crystal-field interaction or single-ion anisotropy, which is often called the spin-1 Blume–Capel model or simply the Blume–Capel model, was first introduced by Blume [21] and independently by Capel [22]. The model has been a subject of many theoretical studies since its introduction [21, 22] nearly 40 years ago because it plays a fundamental role in multicritical phenomena associated with various physical systems, such as multicomponent fluids, ternary alloys, and magnetic systems. The investigations [21, 22] were based on well-known methods in equilibrium statistical physics such as the mean-field approximation, the cluster variation method, the effective field theory, the renormalization-group techniques, and the Monte-Carlo simulations (see, e.g., [23]). While the equilibrium properties of the model have been extensively investigated by many different methods, the nonequilibrium properties of the model have not been as thoroughly explored. As in Ref. [20], Fiig et al. [24] used dynamic Monte-Carlo simulations to study a dynamic behavior of metastable states in the Blume–Capel model and found that the decay of a particular metastable state might happen either directly or via a succession of separate steps, depending on the availability and relative stability of a second metastable state intermediate between the initial one and the equilibrium phase. Manzo and Olivieri [25] have used this model to study the metastability and nucleation by also using the dynamic Monte-Carlo simulations. Ekiz et al. [26] have studied the dynamics of the Blume–Capel model using the path probability method with point distribution [27] in order to investigate how to obtain the metastable phases with long-range order parameters and also to see the "flatness" property of the metastable state and the unstable state. They have also calculated the phase transitions of the metastable and the unstable branches of the order parameters besides the stable branches and presented the complete phase diagram.

The Hamiltonian of the spin-1 Blume–Capel model is given by

$$\mathcal{H} = -J \sum_{\langle ij \rangle} S_i S_j - D \sum_i S_i^2 - H \sum_i S_i, \qquad (1)$$

where S_i take the values ± 1 or 0 at each site i of a lattice and $\langle ij \rangle$ indicates summation over all pairs of nearest-neighbor sites; J is the bilinear exchange interaction parameter; D is the crystal-field interaction or a single-ion anisotropy, and H is a time-dependent external oscillating magnetic field: $H(t) = H_0 \cos \omega t$, H_0 and $\omega = 2\pi\nu$ are the amplitude and the angular frequency of the oscillating field. The system is in contact with an isothermal heat bath at absolute temperature T_A.

We apply the Glauber-type stochastic dynamics to obtain the mean-field dynamic equation of motion. The system evolves according to a Glauber-type stochastic process at a rate of $1/\tau$ transitions per unit time. We define $P(S_1, S_2, \ldots, S_N; t)$ as the probability that the system has the S-spin configuration, $S_1, S_2, \ldots, S_N$, at time t. The time dependence of this probability function is assumed to be governed by the master equation that describes the interaction between spins and heat bath and can be written as

$$\frac{d}{dt}P(S_1,S_2,\ldots,S_N;t) = \\ = -\sum_i \left(\sum_{S_i\neq S_i'} W_i(S_i\to S_i')\right)\times \\ \times P(S_1,S_2,\ldots,S_i,\ldots,S_N;t) + \\ + \sum_i \left(\sum_{S_i\neq S_i'} W_i(S_i'\to S_i)\right)\times \\ \times P(S_1,S_2,\ldots,S_i',\ldots,S_N;t), \quad (2)$$

where $W_i(S_i \to S_i')$ is the probability per unit time that the ith spin changes from the value S_i to S_i', and in this sense the Glauber model is stochastic. Because the system is in contact with a heat bath at absolute temperature T_A, each spin can change from the value S_i to S_i' with the probability per unit time

$$W_i(S_i\to S_i') = \frac{1}{\tau}\frac{\exp\left[-\beta\Delta E(S_i\to S_i')\right]}{\sum\limits_{S_i'}\exp\left[-\beta\Delta E(S_i\to S_i')\right]}, \quad (3)$$

where $\beta = 1/k_BT_A$, k_B is the Boltzmann constant, the sum ranges the three possible values ±1 and 0 for S_i', and

$$\Delta E(S_i\to S_i') = \\ = -(S_i'-S_i)\left(J\sum_{\langle j\rangle} S_j + H\right) - (S_i'^2 - S_i^2)D \quad (4)$$

gives the change in the energy of the system when the S_i spin changes. The probabilities satisfy the detailed balance condition

$$\frac{W_i(S_i\to S_i')}{W_i(S_i'\to S_i)} = \frac{P(S_1,S_2,\ldots,S_i',\ldots,S_N)}{P(S_1,S_2,\ldots,S_i,\ldots,S_N)}. \quad (5)$$

Substituting the possible values of S_i, we obtain

$$\begin{aligned} W_i(1\to-1) &= W_i(0\to-1) = \\ &= \frac{1}{\tau}\frac{\exp(-\beta D)}{2\,\mathrm{ch}(\beta a)+\exp(-\beta D)}, \\ W_i(1\to-1) &= W_i(0\to-1) = \\ &= \frac{1}{\tau}\frac{\exp(-\beta a)}{2\,\mathrm{ch}(\beta a)+\exp(-\beta D)}, \\ W_i(0\to1) &= W_i(-1\to1) = \\ &= \frac{1}{\tau}\frac{\exp(\beta a)}{2\,\mathrm{ch}(\beta a)+\exp(-\beta D)}, \end{aligned} \quad (6)$$

where $a = J\sum\limits_{\langle j\rangle} S_j + H$. We note that because $W_i(S_i \to S_i')$ is independent of S_i, we can write $W_i(S_i \to S_i') = W_i(S_i')$. Then the master equation becomes

$$\frac{d}{dt}P(S_1,S_2,\ldots,S_N;t) = \sum_i \left(\sum_{S_i'\neq S_i} W_i(S_i')\right)\times \\ \times P(S_1,S_2,\ldots,S_i,\ldots,S_N;t) + \\ + \sum_i W_i(S)\left(\sum_{S_i'\neq S_i} P(S_1,S_2,\ldots,S_i',\ldots,S_N;t)\right). \quad (7)$$

Because the sum of probabilities is normalized to unity, by multiplying both sides of Eq. (7) by S_k and taking the average, we obtain

$$\tau\frac{d}{dt}\langle S_k\rangle = -\langle S_k\rangle + \\ + \left\langle \frac{2\,\mathrm{sh}\,\beta\left[J\sum\limits_{\langle j\rangle} S_j + H\right]}{2\,\mathrm{ch}\,\beta\left[J\sum\limits_{\langle j\rangle} S_j + H\right] + \exp(-\beta D)}\right\rangle, \quad (8)$$

or, in terms of the mean-field approach,

$$\tau\frac{d}{dt}\langle S\rangle = -\langle S\rangle + \\ + \frac{2\,\mathrm{sh}\,\beta\left[Jz\langle S\rangle + H_0\cos\omega t)\right]}{2\,\mathrm{ch}\,\beta\left[Jz\langle S\rangle + H_0\cos\omega t\right] + \exp(-\beta D)}, \quad (9)$$

where z is the coordination number. The system evolves according to the differential equation given by Eq. (9), which can be written as

$$\Omega\frac{d}{d\xi}m = -m + \\ + \frac{\mathrm{sh}\left[(m+h\cos\xi)/T\right]}{\mathrm{ch}\left[(m+h\cos\xi)/T\right] + \exp(-d/T)/2}, \quad (10)$$

where $m = \langle S\rangle$, $\xi = \omega t$, $\Omega = \tau\omega$, $T = (\beta zJ)^{-1}$, $d = D/zJ$, and $h = H_0/zJ$. We fix $z = 4$ and $\Omega = 2\pi$.

3. DYNAMIC PHASE TRANSITION POINTS AND PHASE DIAGRAMS

In this section, we first solve the mean-field dynamic equation and present the behavior of average order parameters in a period as a function of the reduced temperature. As a result, the DPT points are calculated. For these purposes, we first have to study the stationary solutions of the dynamic equation, given

in Eq. (10), when the parameters T, d, and h are varied. The stationary solution of Eq. (10) is a periodic function of ξ with period 2π. Moreover, it can be one of two types according to whether it has or does not have the property

$$m(\xi + \pi) = -m(\xi). \tag{11}$$

A solution that satisfies Eq. (11) is called a symmetric solution, which corresponds to a paramagnetic (P) solution. In this solution, the average magnetization $m(\xi)$ oscillates around the zero value and is delayed with respect to the external magnetic field. The second type of solution, which does not satisfy Eq. (11), is called nonsymmetric solution and corresponds to a ferromagnetic (F) solution. In this case, the magnetization does not follow the external magnetic field, but instead of oscillating around a zero value, it oscillates around a nonzero value. These facts are seen explicitly by solving Eq. (10) numerically. Equation (10) is solved using the numerical method of the Adams–Moulton predictor corrector method for a given set of parameters and initial values, and is shown in Fig. 1. From Fig. 1, we see that three different solutions exist in the system: the P, F, and coexistence (P+F) solutions, in which the F and P solutions coexist. In Fig. 1*a*, only the symmetric solution is always obtained, and hence we have the P solution, but in Fig. 1*b*, only the nonsymmetric solution is found; therefore, we have the F solution. Neither solution depends on the initial values. On the other hand, in Fig. 1*c*, both the symmetric and nonsymmetric solutions always exist in the system, and hence we have the F+P solution. In this case, the solutions depend on the initial values, seen in Fig. 1*c* explicitly.

Thus, Fig. 1 shows that we have two types of solutions, symmetric and nonsymmetric. Moreover, it displays that the P solution or phase, the F phase, and the F+P phase exist in the system. To see the boundaries between these three regions, we have to calculate DPT points, and then we can present phase diagrams of the system. DPT points are to be obtained by investigating the behavior of the average magnetization in a period, which is also called the dynamic magnetization, as a function of the reduced temperature. Moreover, we also calculate the Lyapunov exponent to verify the stability of a solution and the DPT points.

The average magnetization in a period or the dynamic magnetization M is given by

$$M = \frac{1}{2\pi} \int_0^{2\pi} m(\xi)\, d\xi. \tag{12}$$

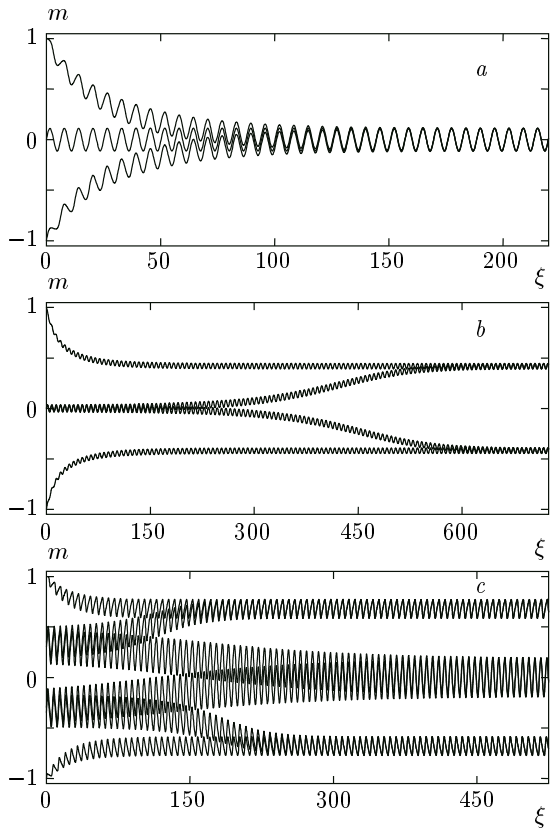

Fig. 1. Time variations of the magnetization m: *a*) exhibiting a paramagnetic phase (P), $d = -0.25$, $h = 0.5$, and $T = 0.75$; *b*) exhibiting a ferromagnetic phase (F), $d = -0.25$, $h = 0.2$, and $T = 0.5$; *c*) exhibiting a coexistence region (F+P), $d = -0.25$, $h = 0.75$, and $T = 0.1$

The behavior of M as a function of the reduced temperature for several values of h and d is obtained by combining the numerical methods of the Adams–Moulton predictor corrector with the Romberg integration; the results are plotted in Fig. 2 together with the Lyapunov exponent λ. Figure 2*a* represents the reduced temperature dependence of the average magnetization M for $h = 0.75$ and $d = 0.25$. In this case, M decreases to zero discontinuously as the reduced temperature increases, and therefore a first-order phase transition occurs at $T_t = 0.2950$. Figures 2*b* and 2*c* illustrate the thermal variations of M for $h = 0.675$ and $d = 0.25$ for two different initial values $M = 1$ and $M = 0$, respectively. In Fig. 2*b*, M decreases to zero continuously as the reduced temperature increases, and therefore the system exhibits a second-order phase transition at $T_c = 0.46$. In Fig. 2*c*, the system undergoes two successive phase transitions. The first is a first-order transition from the

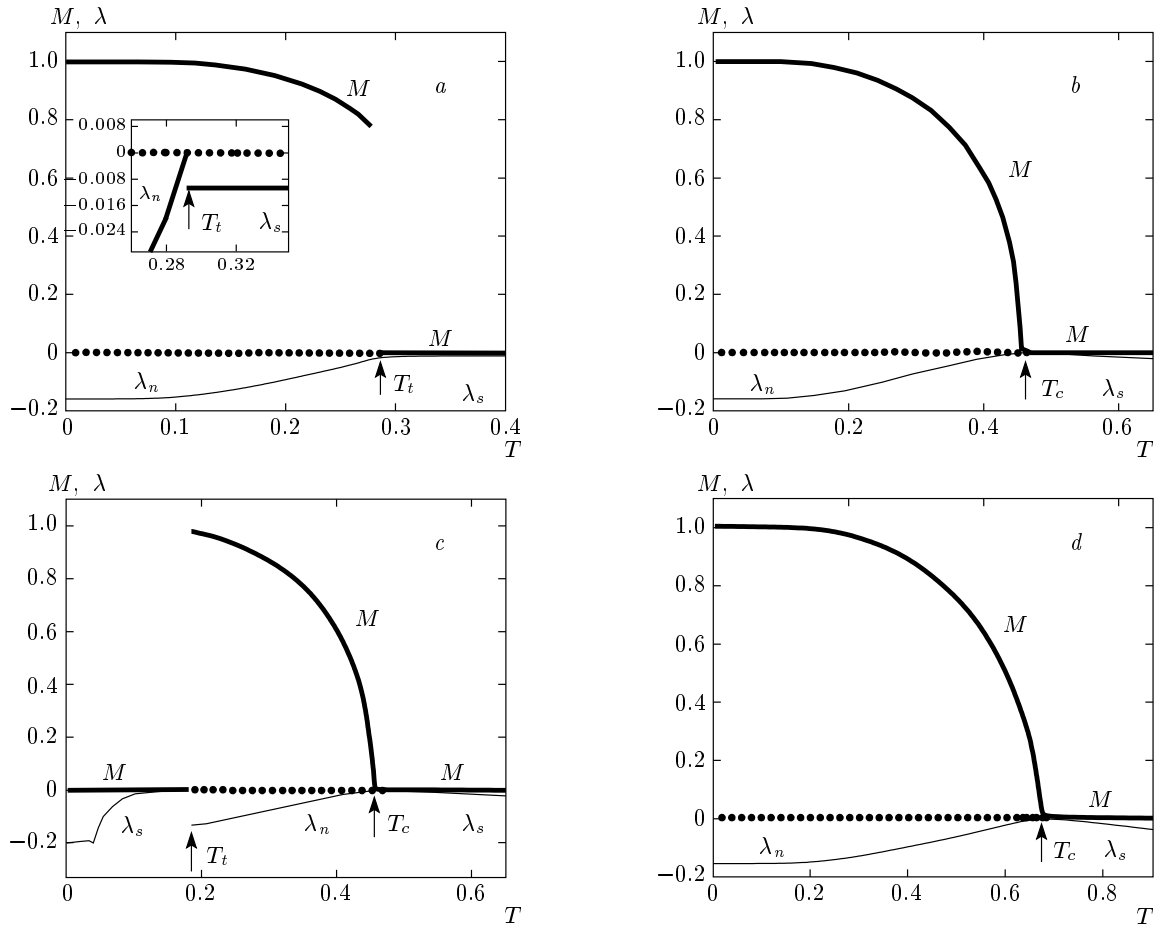

Fig. 2. The reduced temperature dependence of the dynamic magnetization M (the thick solid line) and the Lyapunov exponents λ_s and λ_n (the thin solid line), the subscript "s" indicates a symmetric solution which corresponds to the P phase and "n" indicates a nonsymmetric solution that corresponds to the F phase; T_t and T_c are the first- and second-order phase transition temperatures, respectively. The F+P region exists for $d = 0.25$ and $h = 0.675$. *a*) Exhibiting a first-order phase transition from the F phase to the P phase for $d = 0.25$ and $h = 0.75$; T_t is found to be 0.2950; *b*) exhibiting a second-order phase transition from the F phase to the P phase for $d = 0.25$ and $h = 0.675$; T_c is found to be 0.460; *c*) exhibiting two successive phase transitions, the first one is a first-order phase transition from the P phase to the F phase and the second one is a second-order phase transition from the F phase to the P phase for $d = 0.25$ and $h = 0.675$; T_t and T_c are found to be 0.1950 and 0.460, respectively; *d*) exhibiting a second-order phase transition from the F phase to the P phase for $d = 0.25$ and $h = 0.4$; T_t is found to be 0.6720

P phase to the F phase at $T_t = 0.1950$ and the second is a second-order transition from the F phase to the P phase at $T_c = 0.46$. Finally, Fig. 2*d* shows the behavior of M as a function of the reduced temperature for $h = 0.4$ and $d = 0.25$. It is easily seen that the system undergoes only a second-order phase transition, from the F phase to the P phase at $T_c = 0.6720$.

In order to check the DPT points and verify the stability of solutions, we must calculate the Lyapunov exponent λ. If we write Eq. (10) as

$$\Omega \frac{dm}{d\xi} = F(m, \xi), \tag{13}$$

then the Lyapunov exponent λ is given by

$$\Omega\lambda = \frac{1}{2\pi} \int_0^{2\pi} \frac{\partial F}{\partial m}\, d\xi. \tag{14}$$

The solution is stable when $\lambda < 0$. The behavior of the Lyapunov exponent as a function of temperature is also shown in Fig. 2, thin lines (λ_s and λ_n are the Lyapunov exponents associated with the symmetric and nonsymmetric solutions). If λ_s and λ_n increase

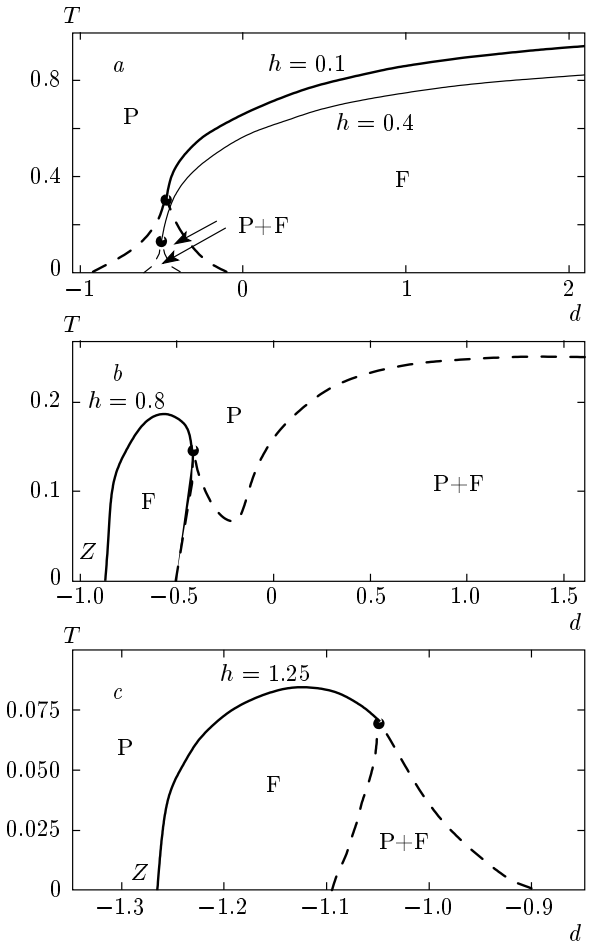

Fig. 3. Phase diagrams of the Blume–Capel model in the (T, d) plane. The P, F, and F+P phase regions are found. Dashed and solid lines represent the dynamic first- and second-order phase boundaries, respectively, the dynamic tricritical points are indicated with solid circles, and Z is the dynamic zero-temperature critical point

to zero continuously as the temperature approaches the phase transition temperature, the temperature, at which $\lambda_n = \lambda_s = 0$, is the second-order phase transition temperature T_c. On the other hand, if one of the λ increases to zero discontinuously and the other λ increases to zero continuously as the temperature approaches the phase transition temperature, the temperature, at which the discontinuity first occurs for one of the λ and the other $\lambda = 0$, is the first-order phase transition temperature T_t. Moreover, if we compare the behavior of M and λ in Fig. 2, we see that T_t and T_c found by using both calculations are exactly the same.

We can now obtain the phase diagrams of the system and the calculated phase diagrams are presented in Fig. 3. One of the most interesting behavior of the phase diagram is that the P phase always exists at low values of T and high negative values of d. The reason can be seen analytically from Eq. (10) as follows. When d takes negative values and increases, the second term in the right-hand side of Eq. (10) disappears. Thus, the solution for the time-dependent magnetization becomes $m(\xi) \propto \exp(-\xi/\Omega)$. As $\xi \to \infty$, the stationary solution for $m(\xi)$ always corresponds to the paramagnetic solution or phase, and hence the dynamic magnetization M vanishes.

As seen in Fig. 3, we have obtained three main different phase diagram topologies according to the values of the reduced external magnetic field amplitude h.

1. For $0 < h \leq 0.6562$, the phase diagram is presented for $h = 0.1$ and $h = 0.4$ in Fig. 3*a*. The system exhibits a dynamic tricritical point, where both first-order phase transition lines merge, and signals change from a first- to a second-order phase transitions. At the temperature higher than the dynamic tricritical point temperature, the dynamic phase boundary between the P phase and F phase is always of a second order. The dynamic phase boundaries between the P and the P+F phases and the P+F and the F phases are always of a first-order for the temperature lower than the dynamic tricritical temperature. Moreover, as the h values increase, a dynamic tricritical point occurs at low temperatures and the F+P region shrinks, as can be seen in the figure. The topology of this phase diagram can be readily obtained from the phase diagrams in Figs. 7*a* and 7*b* in Ref. [20].

2. For $0.6562 < h \leq 0.9828$, shown in Fig. 3*b* for $h = 0.8$, the phase diagram exhibits the dynamic tricritical point and the dynamic zero-temperature critical point Z. For the high negative values of d, the system undergoes a second-order phase transition, which separates the P phase from the F phase. For the low negative values of d, a second-order transition occurs at high temperatures and a first-order transition appears at low temperatures; the second-order line separates the F phase from the P phase and the first-order line separates the F phase from the F+P phase, seen in the figure. Moreover, for very low negative values of d and also for all positive values of d, the system always undergoes a first-order phase transition that separates the F+P phase from the P phase. The topology of this phase diagram can also be obtained from the previous (h, T) phase diagrams, namely Figs. 7*c* and 7*d* in Ref. [20], except the occurrence of a dynamic zero-temperature critical point Z. The occurrence of this surprising or unexpected result is elucidated at the end of this section.

3. For $h > 0.928$, the phase diagram was constructed for $h = 1.25$, as shown in Fig. 3*c*. The phase diagram is similar to the one in Fig. 1*b*, except the following two differences: (i) for positive d values, the system always exhibits the P phase, and hence does not undergo any phase transition; (ii) the first-order phase transition line occurs for high values of d, separates the F phase from the F+P phase (Fig. 3*b*), terminates at zero temperature, and separates the F phase from the F+P phase (Fig. 3*c*). Hence, the P phase always occurs for high values of d and very low values of T. The topology of this phase diagram can also be obtained from the phase diagram in Fig. 7*e* in Ref. [20], except for the occurrence of a dynamic zero-temperature critical point Z. The occurrence of this surprising or unexpected result is also elucidated at the end of this section.

Finally, it is worthwhile to mention that we can see the surprising result in Figs. 3*b* and 3*c* that a dynamic zero-temperature critical point Z appears in these figures, although such a Z point was not to be expected from the previous (h, T) phase diagrams, shown in Figs. 7*c*–*e* in Ref. [20]: another dynamic tricritical point instead of a dynamic zero-temperature critical point Z. This unexpected result can be elucidated by studying the phase diagrams in Figs. 3*b* and 3*c* and considering the previous (h, T) phase diagrams in Figs. 7*c*–*e* in Ref. [20]. In the previous (h, T) phase diagrams, the P, F, and P+F phases exist for low values of T including the absolute zero temperature and the dynamic phase boundary between the P and F phases is always a second-order phase transition line. It has a bulge for a certain range of T, suggesting the occurrence of some sort of a reentrant phenomenon. In Figs. 3*b* and 3*c*, the second-order phase transition line between the P and F phases should start at the Z point, because the P phase occurs at absolute zero, seen in previous (h, T) phase diagrams, and terminates at the dynamic tricritical point where the second-order phase transition line turns to a first-order line; and because the P phase always occurs for high values of T and the dynamic phase boundary between the P and P+F phases is a first-order line. Therefore, this new and surprising result cannot be readily obtained from only the previous (h, T) phase diagrams and it can be understood after calculating and presenting the phase diagrams in the (T, d) plane.

4. CONCLUSIONS

Within the mean-field approach, we have analyzed stationary states of the kinetic spin-1 Blume–Capel model in presence of a time-dependent oscillating external magnetic field. We use a Glauber-type stochastic dynamics to describe the time evolution of the system. The dynamic phase transition (DPT) points are obtained by investigating the behavior of the dynamic magnetization as a function of the reduced temperature. Phase diagrams are presented in the (T, d) plane. We found that the behavior of the system strongly depends on the values of h; three fundamental types of phase diagrams, where the P, F or the P+F phases occur that depend on values of h, are found. Moreover, the system always exhibits a dynamic tricritical point. For $h > 0.6562$, the system also exhibits a dynamic zero-temperature critical point Z, which is unexpected and cannot be readily obtained from only the previous (h, T) phase diagrams [20]. This unexpected result can be elucidated by studying the phase diagrams in Figs. 3*b* and 3*c* and with considering the previous (h, T) phase diagrams. The stability of the solutions and the DPT points are checked by calculating the Lyapunov exponents.

Finally, we also mention that experimental evidence for the DPT has been found in highly anisotropic (Ising-like) and ultrathin Co/Cu(001) ferromagnetic films [18] by the surface magneto-optic Kerr effect and in ferroic systems (ferromagnets, ferroelectrics and ferroelastics) with pinned domain walls [19]. However, the dynamic phase boundary and the nature (continuous/discontinuous) of the transition have not been studied in detail. We hope that our detailed theoretical investigation, especially of the dynamic phase boundary and the nature of the transition, may shed some light or explanation while the detailed experimental studies will be done with the above systems or new systems.

This work was supported by the Scientific and Technological Research Council of Turkey (TÜBİTAK), Grant № 105T114, and Erciyes University Research Funds, Grant № FBA-06-01.

REFERENCES

1. H. E. Stanley, *Introduction to the Phase Transitions and Critical Phenomena*, Oxford Univ. Press, Oxford (1971); S. K. Ma, *Modern Theory of Critical Phenomena*, W. A. Benjamin, Inc, Reading (1976).

2. T. Tomé and M. J. de Oliveira, Phys. Rev. A **41**, 4251 (1990).

3. J. F. F. Mendes and E. J. S. Lage, J. Stat. Phys. **64**, 653 (1991).

4. R. J. Glauber, J. Math. Phys. **4**, 294 (1963).

5. M. Acharyya, Phys. Rev. E **56**, 2407 (1997); A. Chatterjee and B. K. Chakrabarti, Phys. Rev. E **67**, 046113 (2003).

6. S. W. Sides, P. A. Rikvold, and M. A. Novotny, Phys. Rev. Lett. 81, 834 (1998); Phys. Rev. E **59**, 2710 (1999); G. Korniss, C. J. White, P. A. Rikvold, and M. A. Novotny, Phys. Rev. E **63**, 016120 (2001); G. Korniss, P. A. Rikvold, and M. A. Novotny, Phys. Rev. E **66**, 056127 (2002).

7. B. K. Chakrabarti and M. Acharyya, Rev. Mod. Phys. **71**, 847 (1999); M. Acharyya, Int. J. Mod. Phys. C **16**, 1631 (2005).

8. A. Krawiecki, Int. J. Mod. Phys. B **19**, 4769 (2005).

9. M. F. Zimmer, Phys. Rev. E **47**, 3950 (1993); M. Acharyya and B. K. Chakrabarti, Phys. Rev. B **52**, 6550 (1995); M. Acharyya, Phys. Rev. E **58**, 179 (1998); H. Fujisaka, H. Tutu, and P. A. Rikvold, Phys. Rev. E **63**, 036109 (2001).

10. H. Tutu and N. Fujiwara, J. Phys. Soc. Jpn. **73**, 2680 (2004).

11. M. Khorrami and A. Aghamohammadi, Phys. Rev. E **65**, 056129 (2002).

12. H. Jang and M. J. Grimson, Phys. Rev. E **63**, 066119 (2001); H. Jang, M. J. Grimson, and C. K. Hall, Phys. Rev. B **67**, 094411 (2003); Phys. Rev. E **68**, 046115 (2003); Z. Huang, Z. Chen, F. Zhang, and Y. Du, Phys. Lett. A **338**, 485 (2005).

13. T. Yasui, H. Tutu, M. Yamamoto, and H. Fujisaka, Phys. Rev. E **66**, 036123 (2002).

14. E. Machado, G. M. Buendia, P. A. Rikvold, and R. M. Ziff, Phys. Rev. E **71**, 016120 (2005).

15. G. M. Buendia and E. Machado, Phys. Rev. E **58**, 1260 (1998).

16. M. Keskin, O. Canko, and E. Kantar, Int. J. Mod. Phys. C **17**, 1239 (2006); O. Canko, Ü. Temizer, and M. Keskin, Int. J. Mod. Phys. C **17**, 1717 (2006).

17. M. Keskin, O. Canko, and B. Deviren, Phys. Rev. E **74**, 011110 (2006); O. Canko, B. Deviren, and M. Keskin, J. Phys.: Condens. Matter **18**, 6635 (2006); M. Keskin, O. Canko, and M. Kırak, J. Stat. Phys. (2007), in press.

18. Q. Jiang, H. N. Yang, and G. C. Wang, Phys. Rev. B **52**, 14911 (1995); J. Appl. Phys. **79**, 5122 (1996).

19. W. Kleemann, T. Braun, J. Dec, and O. Petracic, Phase Trans. **78**, 811 (2005).

20. M. Keskin, O. Canko, and Ü. Temizer, Phys. Rev. E **72**, 036125 (2005).

21. M. Blume, Phys. Rev. **141**, 517 (1966).

22. H. W. Capel, Physica (Utrecht) **32**, 966 (1966); **33**, 295 (1967).

23. S. Grollau, E. Kierlik, M. L. Rosinberg, and G. Tarjus, Phys. Rev. E **63**, 41111 (2001); A. Du, Y. Q. Yü and H. J. Liu, Physica A **320**, 387 (2003); C. Ekiz, Phys. Lett. A **324**, 114 (2004).

24. T. Fiig, B. M. Gorman, P. A. Rikvold, and M. A. Novotny, Phys. Rev. E **50**, 1930 (1994).

25. F. Manzo and E. Olivieri, J. Stat. Phys. **104**, 1029 (2001).

26. C. Ekiz, M. Keskin, and O. Yalçin, Physica A **293**, 215 (2001).

27. R. Kikuchi, Suppl. Progr. Theor. Phys. **35**, 1 (1966).